*Chemistry - Methods*

Chemistry—Methods

Chemistry Europe
European Chemical Societies Publishing

RESEARCH ARTICLE OPEN ACCESS

# The Inertness of the Lysozyme Template: Assessing the Structural Impact of Silicification Byproducts and Precursors

Tozivepi Aaron Munyayi[1] | Francesco Bruno[1] | Letizia Fiorucci[1] | Vincenzo Mangini[2] | Francesco Scattarella[2] | Cinzia Giannini[2] | Jose Malanho Da Silva[1] | Giacomo Parigi[1,3] | Angelo Gallo[4] | Enrico Ravera[1,3]

[1]CERM and Department of Chemistry "Ugo Schiff", University of Florence, Sesto Fiorentino, Italy | [2]Institute of Crystallography (IC), National Research Council (CNR), Bari, Italy | [3]Consorzio Interuniversitario Risonanze Magnetiche di Metalloproteine, Sesto Fiorentino, Italy | [4]Department of Chemistry, University of Turin, Turin, Italy

**Correspondence:** Francesco Bruno (francesco.bruno@unifi.it) | Angelo Gallo (angelo.gallo@unito.it) | Enrico Ravera (enrico.ravera@unifi.it)

**Received:** 26 June 2026 | **Revised:** 16 July 2026 | **Accepted:** 20 July 2026

**Keywords:** bioinspiration | biophysics | coacervate | lysozyme | nuclear magnetic relaxation | nuclear magnetic resonance | small-angle X-ray scattering

## ABSTRACT

Bioinspired silica deposition with biomolecular templates offers a sustainable route to producing advanced inorganic materials. The templating agent is usually a polycation. Recent experimental evidence links the templating capability of polycationic polymers to self-assembly, coacervation, or liquid–liquid phase separation processes that precede silica deposition. However, when a polycationic protein is used, there is no evidence of liquid–liquid phase separation and the behavior of folded proteins during the hydrolysis of silicon alkoxides (TMOS/TEOS) remains poorly understood. In this study, we investigate the stability and dispersity of lysozyme in the presence of the alkoxide hydrolysis byproducts (methanol and ethanol) and a nonreactive tetrahedral mimic of orthosilicic acid (pentaerythritol). Using Small-Angle X-ray Scattering (SAXS) and Nuclear Magnetic Resonance (NMR) spectroscopy, we demonstrate that lysozyme retains its fold and monomeric state in the presence of these species, with no evidence of aggregation or unfolding. Furthermore, we show that unlike disordered peptides, lysozyme does not require anions for structural organization, even if some self-interaction in the presence of phosphate or other anions is found to occur. These findings support the previously proposed mechanistic model in which the folded protein provides a robust, preorganized electrostatic scaffold for silica deposition, independent of solvent-induced phase transitions.

## 1 | Introduction

The synthesis of silicon dioxide (silica) by living organisms, such as diatoms and sponges, is a neat example of biological control over inorganic materials. This process occurs under physiological conditions, contrasting sharply with the high temperatures and extreme pH required for industrial silica production. Central to this biomineralization is the role of polycationic biomolecules, which catalyze the polycondensation of orthosilicic acid ($H_4SiO_4$) and guide the morphology of the resulting silica phase.

Diatoms employ long-chain polyamines and specific peptides (e.g., silaffins) to accomplish this task. The mechanism by which these systems catalyze the formation of a condensed silica phase under conditions that would otherwise yield a low-condensation silica gel has been a matter of long debate. Lenoci and Camp suggested that these peptides undergo a phase separation to

Enrico Ravera wants to personally express this dedication. With this work I want to recall my good friend, great scientist, and incredibly curious mind Jean-Nicolas Dumez, whose untimely passing has had a profound impact not only on the Nuclear Magnetic Resonance field at large, but also on my personal Weltanschauung.

effectively achieve the supersaturation of silicic acid [1, 2]. More recently, the work of Becker and Kurzbach at the University of Vienna [3, 4] and Gal at the Weizmann Institute of Science [5, 6] has provided experimental validation of this concept. These experiments and simulations propose that for disordered polyamines and peptides, liquid–liquid phase separation (LLPS), or coacervation, or counteranion-mediated self-assembly is a prerequisite for silica precipitation. LLPS concentrates the organic template and silicic acid into a dense liquid phase where polymerization occurs. Additionally, while silica deposition can also occur under dilute conditions, condensation is more efficient and more closely resembles the biological process when LLPS occurs [7]. A recent paper by Kim and Lee further suggests that preformed vesicles containing polyamines and phosphates can improve the monodispersity of the resulting silica particles [8].

While the biomimetic pathways identified early demonstrate the utility of polycationic and folded proteins as simple templates, the modern paradigm of biological silicification highlights a much more sophisticated, multiscale division of tasks in vivo, where chemical catalysis and architectural patterning are decoupled. In marine sponges, for example, the chemical condensation of orthosilicic acid is catalyzed by silicateins—enzymes structurally homologous to the cysteine protease cathepsin L but evolutionary modified with a nucleophilic serine-histidine active site [9]. However, the intricate, species-specific macro- and mesoscale architectures of these biosilica spicules are dictated by a distinct cytoskeletal component: crosslinked F-actin filaments, termed silactins. These silactins act as dynamic extracellular pattern drivers, guiding the physical shape, branching, and symmetry of the growing spicule [10, 11]. Similarly, in glass sponges (Hexactinellida), the synthesis of exceptionally flexible, meter-long anchoring spicules is templated on a highly hydroxylated fibrillar collagen containing an unusual Gly-3Hyp-4Hyp motif, which is stereochemically predisposed to nucleate and template silica precipitation [12], together with histidine-rich protein [13]. Beyond proteinaceous templates, structurally resilient aminopolysaccharides form critical biocomposite scaffolds. Both poriferan [14, 15] and diatom [16] biosilica are heavily reinforced by chitin networks. Centric diatoms like Thalassiosira pseudonana utilize membrane-bound chitin synthases to extrude highly crystalline external β-chitin fibers for buoyancy regulation, while maintaining a more amorphous internal chitin-protein network within the cell wall [17] to serve as a physical blueprint during cell division. Collectively, these natural biosilica architectures illustrate that biological glass growth relies on a complex coordination of enzymatic catalysts and structural matrices (silactins, hydroxylated collagen, and chitin scaffolds) to achieve precise hierarchical order. Decoupling these localized kinetic and physical interactions remains a central challenge in biomimetic materials chemistry, making the structural and mechanical characterization of stable in vitro protein templates highly relevant for synthetic materials engineering.

Based on the pioneering work by Coradin, Durupthy, and Livage that demonstrated that charged peptides achieved "bioinspired silicification" [18], Coradin, Coupé, and Livage in 2003 [19] and Luckarift, Dickerson, Sandhage, and Spain in 2006 [20] showed that folded globular proteins, such as lysozyme, can template silica formation. Lysozyme is less efficient than poly-homopeptides like poly-L-lysine [21], however, it is much less expensive [22]. Utilizing the colorimetric silicomolybdic acid spectrophotometric assay to track the consumption of monomeric orthosilicic acid during the early oligomerization stages [23], Coradin, Eglin, and Livage outlined systematic differences in catalytic efficiency and morphogenetic pathways between linear, flexible polypeptides and rigid, highly structured globular proteins like hen egg white lysozyme (HEWL) [18, 19]. Belton et al. proved that for homopolymeric polylysine and its oligomeric counterparts (lys)n, the silicification kinetics are strongly dependent on chain length, exhibiting a critical transitional threshold between the trimer (lys)3 and tetramer (lys)4; the tetramer serves as the minimal chain length capable of being physically incorporated into the growing silica precipitate, resulting in exponentially accelerated apparent third-order condensation rates and modified pore structures [23].

In spite of the technological appeal of a synthetic route that relies upon the use of lysozyme as a relatively inexpensive precursor [22, 24], the role and the structural fate of the protein in this synthesis remained largely unexplored until recently.

The structural, orientational, and mechanistic roles of HEWL in templating bioinspired silica composites have been comprehensively characterized across three studies. Utilizing solid-state nuclear magnetic resonance (NMR) spectroscopy, small-angle X-ray scattering (SAXS), and scanning electron microscopy (SEM), it was demonstrated that lysozyme remains in intimate contact with the silica matrix without establishing covalent or electrostatic bonds; instead, approximately 80% of the protein is sterically trapped within a "silica cage" during particle formation while fully preserving its native-like tertiary fold, leaving only 20% interacting with the outer surface via electrostatic forces [25]. Preservation of the native fold was established also earlier through NMR and other spectroscopic techniques [26, 27]. Subsequent work using spin-label-based electron paramagnetic resonance (EPR) spectroscopy added crucial spatial resolution to this interface, revealing that a large portion of the protein exhibits a distinct orientational preference by selectively pointing its high-surface charge density patches directly toward the silica material surface [28]. Finally, molecular simulations uncovered the underlying kinetic driving forces of this composite formation: nonreactive classical molecular dynamics (MD) simulations demonstrated that the protein templates the material via an electrostatic pooling mechanism, wherein orthosilicic acid precursors physically cluster around the protein surface, markedly increasing the local precursor concentration near specific highly charged residues (such as Arg-73 and Lys-96/97) and surface patches to drive the polycondensation reaction [29]. In a further study, we have investigated the role of charged aminoacid sidechains, revealing that the activation barrier is not altered significantly nor by the sidechains themselves, nor by the intervening water molecules [30].

Under the typical silicification conditions, lysozyme does not appear to undergo aggregation coacervation or LLPS [25, 31]. The conditions required for lysozyme phase separation are actually quite far removed from the physiological ones [32]. This seemingly contradictory situation can be resolved by considering that proteins effectively behave as colloids [33], in the present case harboring charged and hydrogen-bonding

residues at relatively high local concentration. This hypothesis is corroborated by some recent computational works [29, 30].

However, the chemical environment of in vitro bioinspired silicification is complex. Common laboratory precursors, tetramethyl orthosilicate (TMOS) and tetraethyl orthosilicate (TEOS), release significant amounts of methanol and ethanol, respectively, upon hydrolysis (up to 4 times the amount of silicic acid that is formed - "4 equivalents per mole"). Additionally, the transient formation of reactive silicic acid species presents a unique chemical interface with the protein. It is therefore critical to determine whether the "active" template is the native protein itself or a species structurally perturbed by the accumulation of these chemicals.

In this work, we decouple the effects of hydrolysis byproducts from the polymerization process. We systematically monitor the structural integrity of lysozyme in the presence of methanol and ethanol, and we employ pentaerythritol as a nonpolymerizing steric mimic of orthosilicic acid. We also compare these results with the behavior of disordered peptides, specifically examining the role of phosphate ions. While phosphate is essential for the supramolecular assembly of silaffin-derived peptides (RRIL motifs) [3], we assess its impact on lysozyme structure using a combination of biophysical techniques.

## 2 | Results and Discussion

### 2.1 | Robustness of the Lysozyme Fold Against Hydrolysis Byproducts

The hydrolysis of TMOS and TEOS releases 4 equivalents of methanol or ethanol, respectively, for every mole of silica precursor. To validate lysozyme as a stable template, it is essential to rule out solvent-induced denaturation or oligomerization. High concentrations of short-chain alcohols are well-documented to perturb the native state of lysozyme, driving the transition toward α-helix-rich denatured conformations and inducing aggregation through disruption of hydrophobic interactions [34, 35]. However, these phenomena are strictly threshold dependent, typically requiring ethanol concentrations exceeding 60% (v/v) to overcome the protein's intrinsic electrostatic repulsion [34, 35]. In the regime relevant to our synthesis (400 mM, below 2% v/v), the system operates safely within both kinetic and thermodynamic stability limits. For instance, in 100 mM Tris-HCl, 400 mM methanol, the denaturation temperature of lysozyme is found to be around 69 °C, within the typical range observed for this protein (see Supporting Information for the fluorescence tests). Under these dilution conditions, the native hydration shell and tertiary structure of lysozyme are preserved. Moreover, static light scattering studies indicate that low concentrations of alcohols (<5%) can actually increase protein–protein repulsion [36], reinforcing the structural stability of the monomeric template and minimizing the risk of solvent-induced phase separation or precipitation. To experimentally assess the impact of methanol or ethanol at synthesis-relevant concentrations, we collected SAXS profiles of lysozyme (10 mg/mL) in the absence (Figure 1, cyan) and in the presence of 400 mM methanol (Figure 1, red) and ethanol (Figure 1, green).

As shown in Figure 1, the scattering curves of lysozyme in the presence of alcohols are essentially superimposable to the buffer-only control and the reconstructed pair distribution $p(r)$ remains constant within experimental error. These results indicate that the concentrations of alcohol generated during sol–gel processing do not significantly perturb the tertiary structure of the protein, nor the potential oligomeric state of the protein.

### 2.2 | Pentaerythritol as a Probe for Tetrahedral Geometry Recognition

A key question in biosilicification is whether the protein template specifically recognizes the geometry of the monomeric building block. In a previous work, we observed a tetrahedral titanium species interacting with the sidechain of arginine 14 (Arg14-R14) [31] and MD simulations indicate clustering of orthosilicic acid near charged surface patches [29]. However, there is no stable structural analog of orthosilicic acid, i.e., a stable tetrahedral silicon species capable of hydrogen bonding. To model this species without interference from polycondensation, we utilized pentaerythritol ($C(CH_2OH)_4$). Its molecular size and multiple —OH functionalities confer a polar scaffold with low-to-moderate polarizability that approximates the spatial distribution of silanol groups on silicic acid, enabling qualitative insights into how hydroxyl-rich species interact with charged and polar protein surfaces.

SAXS analysis of lysozyme in the presence of 100 mM pentaerythritol revealed no detectable changes in the scattering profile compared to the native protein (Figure 2). The only difference, a slight reduction in scattering, is likely not significant and may reflect a reduced contrast between the protein surface and the bulk solvent, which could suggest a weak interaction of pentaerythritol with the protein surface.

This interaction was further probed using diffusion ordered spectroscopy (DOSY). In the sample containing pentaerythritol, the translational diffusion of lysozyme is reduced by roughly 10%, consistent with the inclusion of pentaerythritol in the hydration layer of the protein, in agreement with the SAXS observations. Importantly, DOSY data do not indicate the formation of stable protein small molecule complexes on the NMR timescale.

A similar reduction in the translational diffusion coefficient of lysozyme is observed when sulfate or tetrafluoroborate is added to the solution. This likely reflects an increase in the hydrogen-bonding tendency of the protein when the hydrogen-bonding capable species are added. The implications of these findings for the role of phosphate will be discussed in the following section.

The diffusion coefficients obtained from the fits of the DOSY profiles in the aliphatic region of the protein spectrum are reported in Table 1.

### 2.3 | The Role of Phosphate: Structural Assembly or Solvation

Previous studies by Strobl et al. demonstrated that, for disordered peptides containing the RRIL motif, phosphate ions are strictly

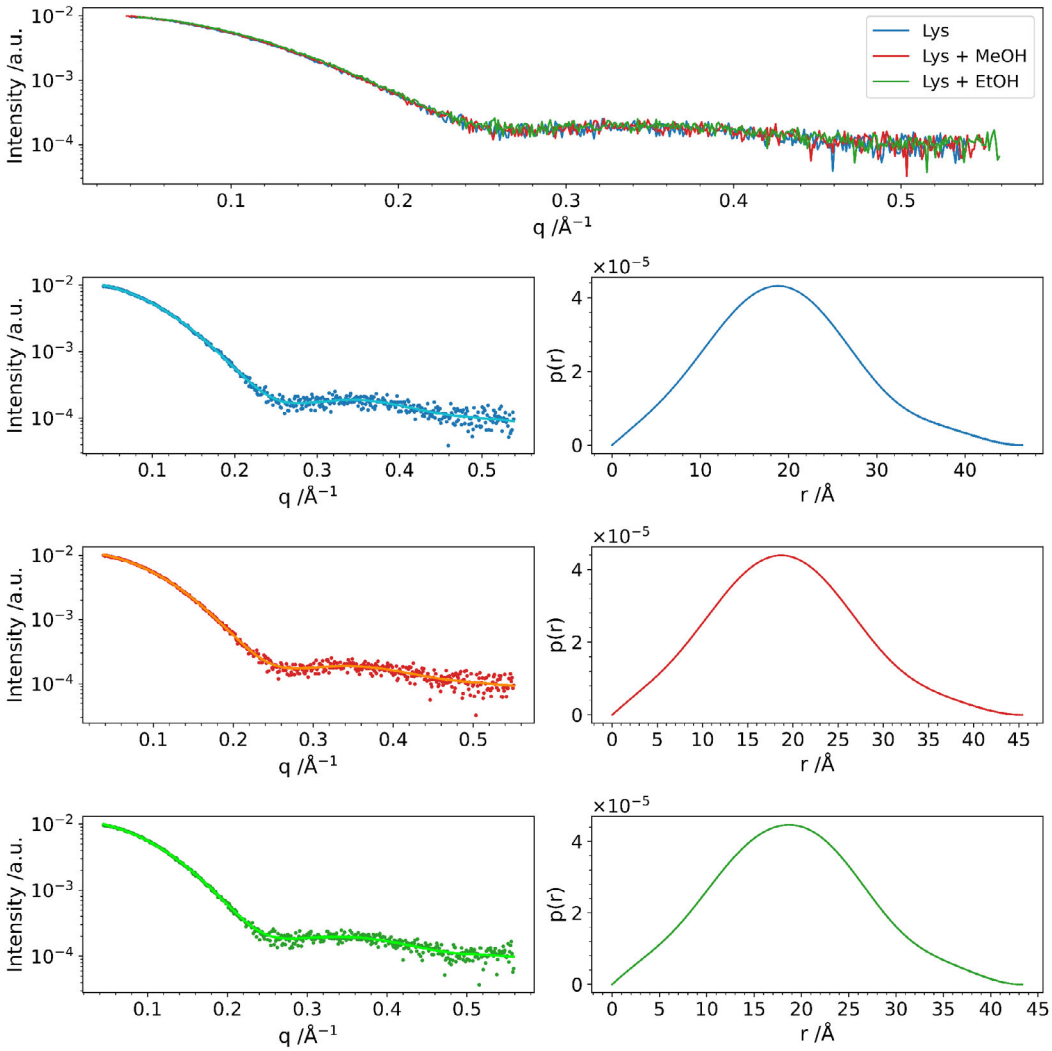


**FIGURE 1** | SAXS profiles of lysozyme (10 mg/mL) in Tris buffer (control), compared with lysozyme (10 mg/mL) at the same concentration in the presence of MeOH and EtOH. (Top) Overlay of the scattering profiles for all samples. (Cyan) Lysozyme in Tris buffer. (Red) Lysozyme in the presence of MeOH. (Green) Lysozyme in the presence of EtOH. The lower panels show the individual scattering curves together with the reconstructed pair distribution $p(r)$.

required for bridging different polycations, driving the self-assembly of the peptide into the supramolecular template necessary for silica precipitation [3]. For this section, the measurements were performed replacing 100 mM Tris buffer with 100 mM phosphate buffer, keeping the pH constant, unless differently specified.

In this case, the SAXS data are not perfectly conclusive, but are still indicative of a different situation.

The SAXS profiles show only a minor difference in the low-$q$ region compared to the Tris-HCl buffer (Figure 3). This variation corresponds to a slight increase in the apparent Rg. The SAXS data of the sample without phosphate are perfectly compatible with the X-ray model of lysozyme, 6F1O [39], the X-ray structure that best reproduces lysozyme solution NMR data [40]. On the contrary, the SAXS data obtained in the presence of phosphate require a higher contrast with respect to what is obtained with the model of phosphate-bound lysozyme (6F1P).

There are two reasonable explanations for this observation. The first, more straightforward, is that the protein undergoes a minor oligomerization. This would be perfectly in line with what was observed in the early stages of crystallization [41]. Following the same scheme as the one proposed by Marchenkova et al., the data can be fit satisfactorily using OLIGOMER [42, 43] if the percentages of the monomer/dimer/octamer species are $91.2 \pm 0.8/6.9 \pm 0.9/1.9 \pm 0.2$, whereas the data in Tris-HCl buffer are fully consistent with the monomeric structure 6F1O. This explains the shift in the peak of the $p(r)$ distribution (Figure 3) and the extent of the curve at larger distances. An alternative explanation is a change in the scattering contrast of the protein arising from the increased presence of phosphate ions in the first hydration shell of the protein relative to the bulk solution, rather than a change in the protein aggregation state. This would be reflected in similar features in the $p(r)$ distribution function.

The interaction between lysozyme and phosphate was also probed through nuclear magnetic resonance dispersion (NMRD), where the solvent relaxation rates are measured at

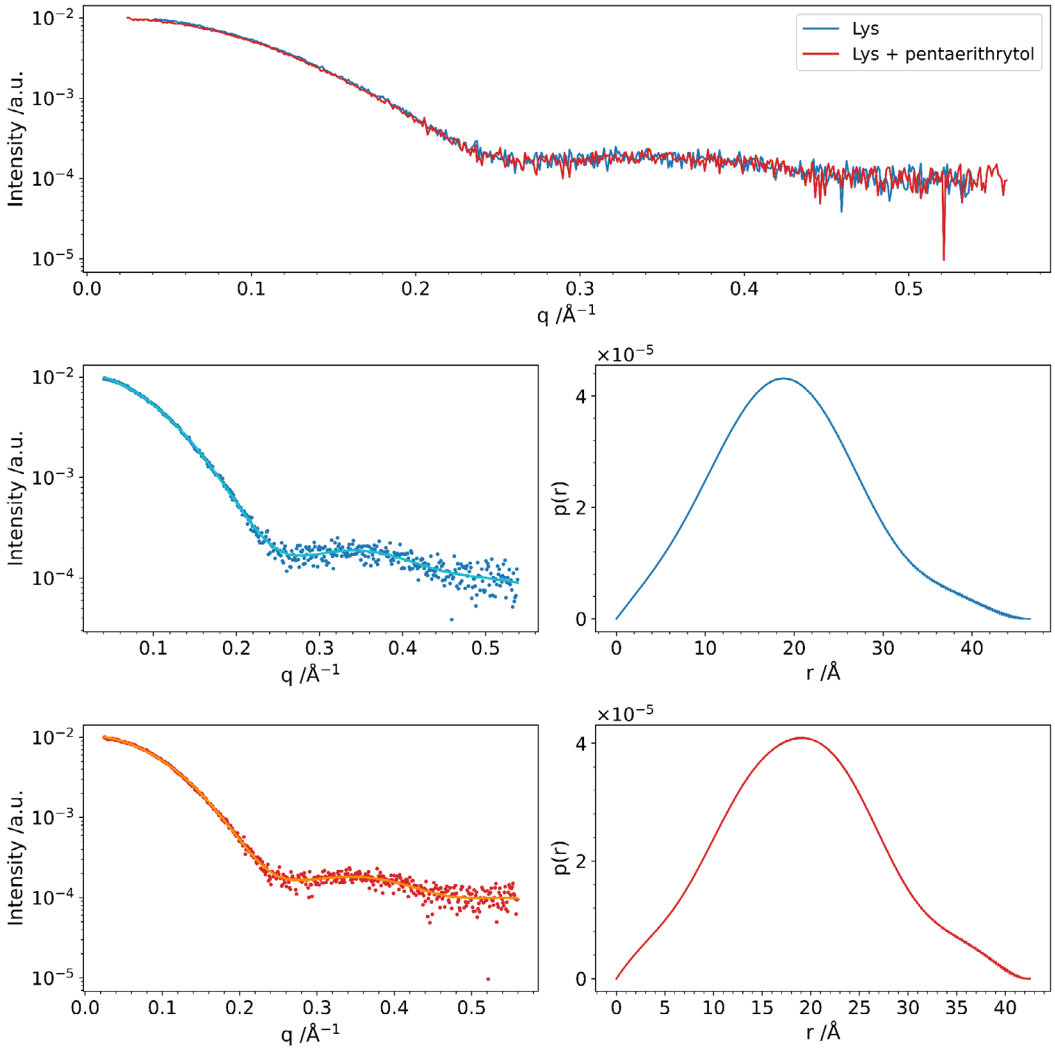


**FIGURE 2** | SAXS profiles of lysozyme (10 mg/mL) in Tris buffer (control) compared with lysozyme (10 mg/mL) in the presence of pentaerythritol. (Top) Overlay of the scattering profiles for all samples. (Cyan) Lysozyme in Tris buffer, same as Figure 1. (Red) Lysozyme in the presence of pentaerythritol. The lower panels show the individual scattering curves together with the reconstructed $p(r)$ distributions.

**TABLE 1** | Diffusion coefficients of lysozyme in the presence of different additives. The fit uncertainty is reported, although the overall experimental uncertainty is expected to be a larger error due to the intrinsic limitations of the technique [37]. The translational diffusion of free lysozyme computed using HullRad [38] is 1.34e-10 with an expected uncertainty of 10%.

| Sample | $D$, $m^2 s^{-1}$ | Fit uncertainty, $m^2 s^{-1}$ |
|---|---|---|
| Lysozyme plain | $1.3388 \times 10^{-10}$ | $1.1 \times 10^{-14}$ |
| Lysozyme + pentaE | $1.2750 \times 10^{-10}$ | $8.3 \times 10^{-15}$ |
| Lysozyme + $BF_4^-$ | $1.24 \times 10^{-10}$ | $1.2 \times 10^{-12}$ |
| Lysozyme + $SO_4^{2-}$ | $1.211 \times 10^{-10}$ | $6.7 \times 10^{-13}$ |

multiple fields and thus can be used to estimate the reorientational correlation time of the solute molecules (Figure 4). The measurements were carried out in both neat buffers but, to minimize the difference among the samples, Tris buffer was used for both samples, but in one of the samples 20 mM phosphate (80/20 Tris/phosphate mixture) were added.

The best fit analysis of the relaxometric profiles using a single correlation time (solid lines) provides $\tau_c$ values of 7.6 ± 0.7 ns for lysozyme in Tris and 10 ± 1 ns in the presence of phosphate (both with and without Tris). Since monomeric lysozyme can be computed [38, 45] to have a reorientation time of ca. 7.5 ± 0.8 ns, this analysis suggests that at pH 7.5 the NMRD data in Tris are consistent with a monomeric form, and in agreement with SAXS. Phosphate appears to increase the content in multimeric species (see SI for discussion), also in agreement with SAXS. If the SAXS-derived weights [41] are used with the computed reorientation times for the monomer, dimer, and octamer (Table S1), the expected average $\tau_c$ evaluates to 9.6 ± 0.7 ns, again in good agreement with the experimental NMRD profile. The shape of the relaxation profiles for lysozyme in Tris with phosphate suggests that the quality of the fit could be improved by introducing a second correlation time through the Lipari–Szabo model-free approach [44, 46, 47]. By fixing the shorter correlation time to 8 ns and leaving the squared-order parameter and the slower correlation time free to optimize, the resulting fits (dotted lines) reveal significant contributions from slower correlation times ranging from 21 ± 16 to 67 ± 22 ns

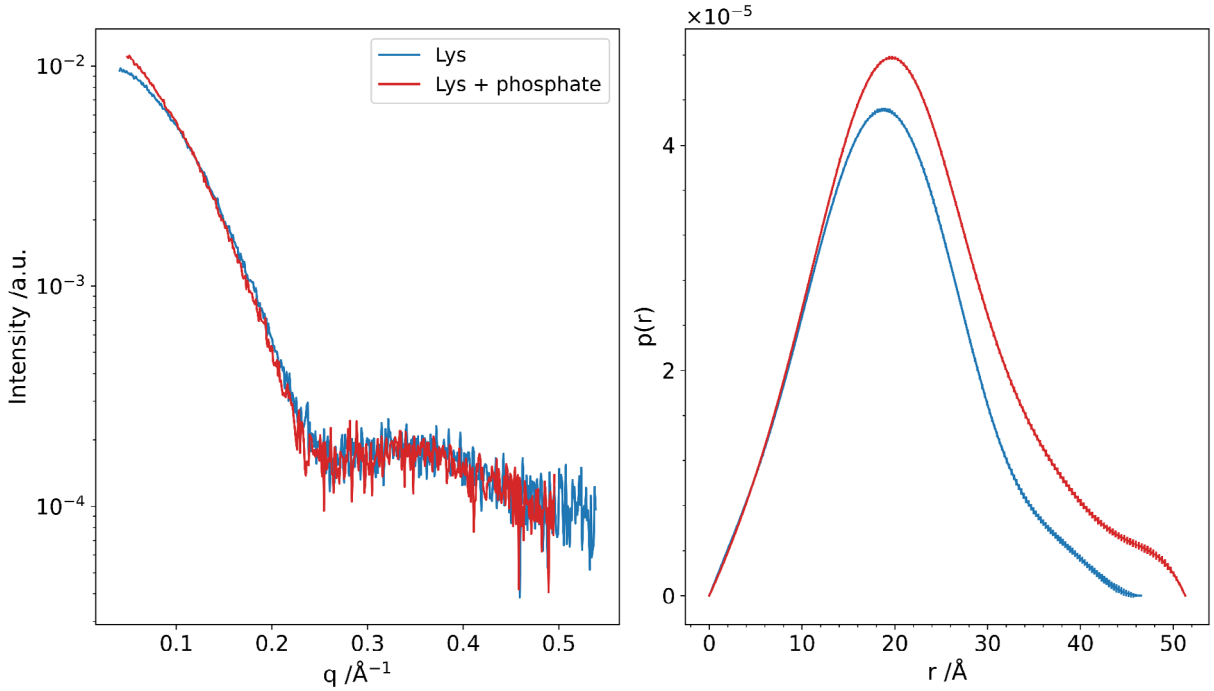


**FIGURE 3** | Comparison of SAXS profiles of lysozyme at 10 mg/ml in the presence (cyan) and in the absence (red) of phosphate. The right panel shows the reconstructed $p(r)$.

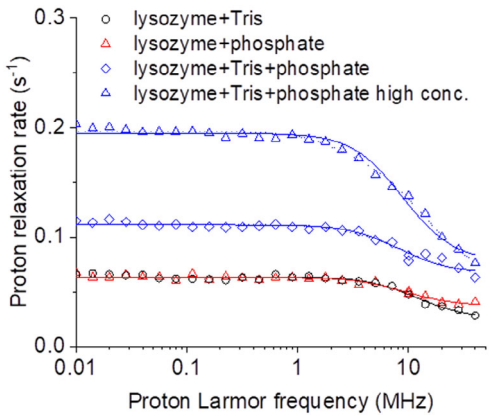


**FIGURE 4** | The NMRD profiles of lysozyme Tris and phosphate containing buffers. Samples were measured in neat Tris buffer, neat Phosphate buffer, and in 80/20 Tris/phosphate buffer mixtures, all at 10 mg/ml. The sample in 80/20 was also repeated at the higher concentration (40 mg/ml as previously reported for the characterization of this protein [44]). The higher relaxation rates of the Tris/phosphate sample at 10 mg/ml are likely originating from a different interaction of solvent protons with the protein protons. The intensity of the profile does not affect the reconstruction of the reorientational motion.

in the high-concentration phosphate sample. Both times are within the experimental uncertainty of the proposed aggregated species (see SI).

Even if aggregation is observed in the presence of phosphate and also of other anions, we should stress that the vast majority of the protein is still found in its monomeric form, and no evidence of LLPS or coacervation is found in these systems.

## 3 | Materials and Methods

### 3.1 | Sample Preparation

#### *3.1.1 | Sample Preparation for SAXS Experiments*

HEWL was dissolved at a concentration of 10 mg/mL in two different buffer systems: 100 mM Tris-HCl (pH 7.5) or 100 mM phosphate buffer (pH 7.5). To investigate alcohol–protein interactions, methanol or ethanol was added to the protein-buffer solutions to obtain a final alcohol concentration of 400 mM. For mimic studies, pentaerythritol was added to the HEWL solutions in both buffer systems to a final concentration of 100 mM. All samples were gently mixed and incubated at 25 °C for 30 min to allow equilibration prior to measurements. All reagents were of analytical grade and purchased from Sigma–Aldrich (St.Louis, MO,USA).

#### *3.1.2 | Sample Preparation NMR Experiments*

HEWL was dissolved at a concentration of 10 mg/mL in 100 mM Tris-HCl (pH 7.5) or 100 mM phosphate buffer (pH 7.5). To investigate alcohol–protein interactions, methanol or ethanol was added to the protein-buffer solutions to obtain a final alcohol concentration of 400 mM. For mimic studies, pentaerythritol was added to the HEWL solutions in both buffer systems to a final concentration of 100 mM.

#### *3.1.3 | Sample Preparation for NMRD Experiments*

HEWL was dissolved at a concentration of 10 mg/mL in 100 mM Tris-HCl (pH 7.5), 100 mM phosphate buffer (pH 7.5), or a mixture of 80 mM Tris-HCl (pH 7.5) and 20 mM phosphate buffer

(pH 7.5). This latter sample was also measured at 45 mg/ml in line with previous studies [44].

### 3.2 | Small-Angle X-Ray Scattering (SAXS)

SAXS measurements were performed at the BioSAXS Laboratory of the ITACA.SB Research Infrastructure, hosted at the CNR Institute of Crystallography (Bari, Italy) [48]. The experiments were carried out using a Xeuss 3.0 h SAXS system (Xenocs, France) equipped with a motorized dual-source stage, including a high-brilliance Ga Liquid Metal-Jet source (Excillum Metaljet D2+, $\lambda = 1.34144$ Å) and a Cu microfocus source (GENIX3D, $\lambda = 1.54189$ Å). Scattered radiation was recorded using an Eiger2 R 1 M detector (DECTRIS), mounted on a vacuum flight tube and movable over a continuous range of sample-to-detector distances (SDD) from 42.5 to 1800 mm, enabling flexible angular coverage and q-range selection.

For the present measurements, the Ga liquid metal-jet source was employed with a SDD of 350 mm, corresponding to a q-range of approximately 0–0.5 $Å^{-1}$. Samples were loaded into a 2 mm BioCube capillary and measured using six consecutive exposures of 300 s each. An offline comparison of successive frames confirmed the absence of radiation-induced sample damage during data acquisition.

The two-dimensional scattering patterns were automatically calibrated and converted into one-dimensional scattering profiles by azimuthal integration using the XSACT software package ("XSACT: X-ray Scattering Analysis and Calculation Tool." xsact.xenocs.com, 2023. SAXS & WAXS data analysis software—Version 2.10). Data reduction and buffer subtraction were performed following standard protocols [48] and resulting data were subsequently analyzed with the program ATSAS (version 4.1.3) [43].

### 3.3 | PFG-NMR Spectroscopy

The DOSY experiments were acquired at a Bruker Avance Neo spectrometer operating at 16.4 T, corresponding to 700 MHz $^1$H Larmor frequency. The spectrometer is equipped with a 5 mm wide-bore BBO probe, water cooled, able to generate gradients up to 735 G/cm.

The experiments were recorded at 298 K by employing a stimulated-echo sequence with bipolar gradients (stebpgp1s19) with the following parameters: $\Delta = 100$ ms, $\delta = 1$ ms, $\tau = 200$ µs, and 90° pulse duration = 19.1 µs.

The obtained spectra were processed and fitted with an in-house script based on the Klassez package [49]. To get the diffusion coefficients, the profiles obtained from the integration of characteristic regions of the spectra were fitted using the Stejskal–Tanner equation modified by Jerschow and Müller [50], as implemented in: https://klassez.readthedocs.io/latest/fit.html#klassez.fit.model_stebp

$$y(g) = \exp\{-D(2\pi\gamma g\delta)^2(\Delta - \delta/3 - \tau - 4p_{90})\}$$

### 3.4 | Nuclear Magnetic Relaxation Dispersion

$^1$H nuclear magnetic relaxation dispersion (NMRD) profiles were recorded with a Stelar SPINMASTER FFC2000 1T fast field cycling relaxometer, operating in the 0.01–40 MHz $^1$H Larmor frequency range. The measurements are affected by an error within ±1%, as obtained in the field cycling experiment from the fit to a monoexponential decay/recovery of the magnetization. The relaxation dispersions are reported as the difference between the relaxation rates measured for the protein samples and the rates of the corresponding buffer solutions. Measurements were performed at 25 °C.

## 4 | Conclusions

Our investigation confirms a fundamental mechanistic distinction between disordered peptides and folded proteins in bioinspired silicification. While silaffin-derived peptides require phosphate-mediated self-assembly to template silica formation, lysozyme acts as a "rigid" scaffold. Its ability to catalyze silica formation is intrinsic to its native fold, which remains stable even in the presence of relatively high concentrations of alcohols released during TEOS/TMOS hydrolysis. The absence of structural reorganization in the presence of the silicic acid mimic pentaerythritol further supports a model in which the protein provides a preorganized electrostatic landscape for catalysis, rather than undergoing dynamic phase separation. This inherent stability simplifies the design of biomimetic silica synthesis, suggesting that folded proteins offer a predictable and robust platform for materials engineering. Interestingly, phosphate also promotes a certain degree of aggregation in this system, but the effect is significantly less pronounced than that observed for short peptides.

#### Acknowledgments

We acknowledge the financial support provided by the MUR – Dipartimenti di Eccellenza 2023–2027 DICUS 2.0 to the Department of Chemistry "Ugo Schiff" of the University of Florence and CH4.0 to the Department of Chemistry of the University of Turin. This project received financial support under the National Recovery and Resilience Plan (NRRP), Mission 4, Component 2, Investment 1.1, Call for Tender No. 1409 published on 14/9/2022 by the Italian Ministry of University and Research (MUR), funded by the European Union NextGenerationEU project titled "Mechanism of Bioinspired Inorganic Oxide Formation" (MInO), CUP D53D23016850001, Grant Assignment Decree No. 1386 adopted on 01/09/2023 by the MUR. The experiments were supported by the project "Potentiating the Italian Capacity for Structural Biology Services in Instruct-ERIC" (ITACA.SB; Project No. IR0000009, CUP B53C22001790006) funded by the European Union NextGenerationEU under MUR call 3264/2021 PNRR M4/C2/L3.1.1. Funding by the Fondazione Cassa di Risparmio di Firenze is also gratefully acknowledged.

Open access publishing facilitated by Universita degli Studi di Firenze, as part of the Wiley - CRUI-CARE agreement.

## Funding

This study was supported by Ministero dell'Università e della Ricerca (Grant D53D23016850001 and B53C22001790006).

## Conflicts of Interest

The authors declare no conflicts of interest.

## Data Availability Statement

The data that support the findings of this study are available from the corresponding author upon reasonable request.

## References

1. L. Lenoci and P. J. Camp, "Self-Assembly of Peptide Scaffolds in Biosilica Formation: Computer Simulations of a Coarse-Grained Model," *Journal of the American Chemical Society* 128 (2006): 10111–10117.

2. L. Lenoci and P. J. Camp, "Diatom Structures Templated by Phase-Separated Fluids," *Langmuir* 24 (2008): 217–223.

3. J. Strobl, F. Kozak, M. Kamalov, D. Reichinger, D. Kurzbach, and C. F. Becker, "Understanding Self-Assembly of Silica-Precipitating Peptides to Control Silica Particle Morphology," *Advanced Materials* 35 (2023): 2207586.

4. F. Kozak, D. Brandis, C. Pötzl, et al., "An Atomistic View on the Mechanism of Diatom Peptide-Guided Biomimetic Silica Formation," *Advanced Science* 11 (2024): 2401239.

5. H. Zhai, T. Bendikov, and A. Gal, "Phase Separation of Oppositely Charged Polymers Regulates Bioinspired Silicification," *Angewandte Chemie International Edition English* 61 (2022): e202115930.

6. H. Zhai, Y. Fan, W. Zhang, N. Varsano, and A. Gal, "Polymer-Rich Dense Phase Can Concentrate Metastable Silica Precursors and Regulate Their Mineralization," *ACS Biomaterials Science & Engineering* 9 (2023): 601–607.

7. P. Biswas, L. Aram, N. Livni, et al., "Macromolecular Condensates as Tunable Scaffolds for Bio-Inspired Silica Hybrids," *Angewandte Chemie International Edition* n/a (n/a): e22966.

8. D.-Y. Kim and C.-S. Lee, "Controlled Biomimetic Silicification in Microdroplets via Spatial Confinement and Synchronized Condensation," *Chemical Engineering Journal* 530 (2026): 173652.

9. K. Shimizu, J. Cha, G. D. Stucky, and D. E. Morse, "Silicatein Alpha: Cathepsin L-Like Protein in Sponge Biosilica," *Proceedings of the National Academy of Sciences of the United States of America* 95 (1998): 6234–6238.

10. H. Ehrlich, A. Voronkina, K. Tabachnick, A. Kubiak, A. Ereskovsky, and T. Jesionowski, "Silactins and Structural Diversity of Biosilica in Sponges," *Biomimetics* 9 (2024): 393.

11. H. Ehrlich, M. Luczak, R. Ziganshin, et al., "Arrested in Glass: Actin Within Sophisticated Architectures of Biosilica in Sponges," *Advanced Science (Weinh)* 9 (2022): e2105059.

12. H. Ehrlich, R. Deutzmann, E. Brunner, et al., "Mineralization of the Metre-Long Biosilica Structures of Glass Sponges Is Templated on Hydroxylated Collagen," *Nature Chemistry* 2 (2010): 1084–1088.

13. K. Shimizu, T. Amano, Md R. Bari, J. C. Weaver, J. Arima, and N. Mori, "Glassin, a Histidine-Rich Protein From the Siliceous Skeletal System of the Marine Sponge Euplectella, Directs Silica Polycondensation," *Proceedings of the National Academy of Sciences* 112 (2015): 11449–11454.

14. H. Ehrlich, M. Maldonado, K. Spindler, et al., "First Evidence of Chitin as a Component of the Skeletal Fibers of Marine Sponges. Part I. Verongidae (demospongia: Porifera)," *Journal of Experimental Zoology Part B: Molecular and Developmental Evolution* 308B (2007): 347–356.

15. H. Ehrlich, M. Krautter, T. Hanke, et al., "First Evidence of the Presence of Chitin in Skeletons of Marine Sponges. Part II. Glass Sponges (Hexactinellida: Porifera)," *Journal of Experimental Zoology Part B: Molecular and Developmental Evolution* 308B (2007): 473–483.

16. E. Brunner, P. Richthammer, H. Ehrlich, et al., "Chitin-Based Organic Networks: An Integral Part of Cell Wall Biosilica in the Diatom Thalassiosira Pseudonana," *Angewandte Chemie International Edition* 48 (2009): 9724–9727.

17. C. A. Durkin, T. Mock, and E. V. Armbrust, "Chitin in Diatoms and Its Association With the Cell Wall," *Eukaryotic Cell* 8 (2009): 1038–1050.

18. T. Coradin, O. Durupthy, and J. Livage, "Interactions of Amino-Containing Peptides With Sodium Silicate and Colloidal Silica: A Biomimetic Approach of Silicification," *Langmuir* 18 (2002): 2331–2336.

19. T. Coradin, A. Coupé, and J. Livage, "Interactions of Bovine Serum Albumin and Lysozyme With Sodium Silicate Solutions," *Colloids and Surfaces B: Biointerfaces* 29 (2003): 189–196.

20. H. R. Luckarift, M. B. Dickerson, K. H. Sandhage, and J. C. Spain, "Rapid, Room-Temperature Synthesis of Antibacterial Bionanocomposites of Lysozyme With Amorphous Silica or Titania," *Small* 2 (2006): 640–643.

21. T. Coradin, P. J. Lopez, C. Gautier, and J. Livage, "From Biogenic to Biomimetic Silica," *Comptes Rendus Palevol* 3 (2004): 443–452.

22. C.-Y. Cheng, M.-Y. Wang, and S.-Y. Suen, "Eco-Friendly Polylactic Acid/Rice Husk Ash Mixed Matrix Membrane for Efficient Purification of Lysozyme From Chicken Egg White," *Journal of the Taiwan Institute of Chemical Engineers* 111 (2020): 11–23.

23. D. Belton, G. Paine, S. V. Patwardhan, and C. C. Perry, "Towards an Understanding of (bio)silicification: The Role of Amino Acids and Lysine Oligomers in Silicification," *Journal of Materials Chemistry* 14 (2004): 2231–2241.

24. R. Curley, J. D. Holmes, and E. J. Flynn, "Can Sustainable, Monodisperse, Spherical Silica Be Produced From Biomolecules? a Review," *Applied Nanoscience* 11 (2021): 1777–1804.

25. F. Bruno, L. Gigli, G. Ferraro, et al., "Lysozyme Is Sterically Trapped Within the Silica Cage in Bioinspired Silica–Lysozyme Composites: A Multi-Technique Understanding of Elusive Protein–Material Interactions," *Langmuir* 38 (2022): 8030–8037.

26. P. A. Mirau, *in Bio-Inspired Nanotechnology: From Surface Analysis to Applications* eds. M. R. Knecht, T. R. Walsh, (Springer, 2014), 95–125.

27. E. Ravera, V. K. Michaelis, T.-C. Ong, et al., "Biosilica-Entrapped Enzymes Studied by Using Dynamic Nuclear-Polarization-Enhanced High-Field NMR Spectroscopy," *ChemPhysChem* 16 (2015): 2751–2754.

28. F. Bruno, L. Gigli, and E. Ravera, "Spin Label Study of the Orientational Preferences of Lysozyme in a Bioinspired Silica Composite," *Journal of Composites Science* 7 (2023): 188.

29. M. Macchiagodena, M. Fragai, A. Gallo, M. Pagliai, and E. Ravera, "The Role of Lysozyme in the Formation of Bioinspired Silicon Dioxide," *Chemistry – A European Journal* 30 (2024): e202401249.

30. J. Lanuza and E. Ravera, "The Impact of Arginine Side Chains on the Mechanism of Polycondensation of Silicic Acid in Bioinspired Mineralization," *Inorganics* 13 (2025): 206.

31. L. Gigli, E. Ravera, V. Calderone, and C. Luchinat, "On the Mechanism of Bioinspired Formation of Inorganic Oxides: Structural Evidence of the Electrostatic Nature of the Interaction Between a Mononuclear Inorganic Precursor and Lysozyme," *Biomolecules* 11 (2021): 43.

32. P. Pyne and R. K. Mitra, "Excipients Do Regulate Phase Separation in Lysozyme and Thus Also Its Hydration," *The Journal of Physical Chemistry Letters* 13 (2022): 931–938.

33. J. Loeb, "The Colloidal Behavior of Proteins," *The Journal of General Physiology* 3 (1921): 557–564.

34. S. Tanaka, Y. Oda, M. Ataka, K. Onuma, S. Fujiwara, and Y. Yonezawa, "Denaturation and Aggregation of hen Egg Lysozyme in Aqueous Ethanol Solution Studied by Dynamic Light Scattering," *Biopolymers* 59 (2001): 370–379.

35. T. Takamuku, T. Haraguchi, R. Sasaki, Y. Hozoji, K. Sadakane, and H. Iwase, "Alcohol-Induced Denaturation of Hen Egg White Lysozyme Studied by Infrared, Circular Dichroism, and Small-Angle Neutron Scattering," *The Journal of Physical Chemistry. B* 128 (2024): 4076–4086.

36. W. Liu, D. Bratko, J. M. Prausnitz, and H. W. Blanch, "Effect of Alcohols on Aqueous Lysozyme–lysozyme Interactions From Static Light-Scattering Measurements," *Biophysical Chemistry* 107 (2004): 289–298.

37. G. A. Morris, *eMagRes* (John Wiley & Sons, Ltd., 2009).

38. P. J. Fleming and K. G. Fleming, "HullRad: Fast Calculations of Folded and Disordered Protein and Nucleic Acid Hydrodynamic Properties," *Biophysical Journal* 114 (2018): 856–869.

39. M. Plaza-Garrido, M. C. Salinas-Garcia, and A. Camara-Artigas, "Orthorhombic Lysozyme Crystallization at Acidic pH Values Driven by Phosphate Binding," *Acta Crystallographica. Section D, Structural Biology* 74 (2018): 480–489.

40. A. Schirò, A. Carlon, G. Parigi, et al., "On the Complementarity of X-Ray and NMR Data," *Journal of Structural Biology: X* 4 (2020): 100019.

41. M. A. Marchenkova, A. S. Boikova, K. B. Ilina, et al., "The Relationship of Precursor Cluster Concentration in a Saturated Crystallization Solution to Long-Range Order During the Transition to the Solid Phase," *Acta Naturae* 15 (2023): 58–68.

42. P. V. Konarev, V. V. Volkov, A. V. Sokolova, M. H. J. Koch, and D. I. Svergun, "PRIMUS - A Windows-PC Based System for Small-Angle Scattering Data Analysis," *Journal of Applied Crystallography* 36 (2003): 1277–1282.

43. D. Franke, T. Gräwert, and D. I. Svergun, "New Features in ATSAS-4, a Program Suite for Small-Angle Scattering Data Analysis," *Journal of Applied Crystallography* 58 (2025): 1027–1033.

44. I. Bertini, M. Fragai, C. Luchinat, and G. Parigi, "1H NMRD Profiles of Diamagnetic Proteins: A Model-Free Analysis," *Magnetic Resonance in Chemistry* 38 (2000): 543–550.

45. Y. Ryabov, J.-Y. Suh, A. Grishaev, G. M. Clore, and C. D. Schwieters, "Using the Experimentally Determined Components of the Overall Rotational Diffusion Tensor to Restrain Molecular Shape and Size in NMR Structure Determination of Globular Proteins and Protein-Protein Complexes," *Journal of the American Chemical Society* 131 (2009): 9522–9531.

46. G. Lipari and A. Szabo, "Model-Free Approach to the Interpretation of Nuclear Magnetic Resonance Relaxation in Macromolecules. 1. Theory and Range of Validity," *Journal of the American Chemical Society* 104 (1982): 4546–4559.

47. G. Lipari and A. Szabo, "Model-Free Approach to the Interpretation of Nuclear Magnetic Resonance Relaxation in Macromolecules. 2. Analysis of Experimental Results," *Journal of the American Chemical Society* 104 (1982): 4559–4570.

48. F. Scattarella, D. Altamura, V. Mangini, et al., "The BioSAXS Laboratory of the ITACA.SB Research Infrastructure," *Journal of Applied Crystallography* (2026, in press), http//doi.org/10.1107/S1600576726007132.

49. F. Bruno, *Automatized Quantitative NMR for Industrial Applications* (University of Florence, 2025).

50. A. Jerschow and N. Müller, "Convection Compensation in Gradient Enhanced Nuclear Magnetic Resonance Spectroscopy," *Journal of Magnetic Resonance* 132 (1998): 13–18.

## Supporting Information

Additional supporting information can be found online in the Supporting Information section.